AD-A084 986 NAVAL RESEARCH LAB WASHINGTON DC F/G 8/3
ON THE MEASUREMENT OF GEOSTROPHIC OCEAN CURRENTS BY (NADIR) SAT--ETC(U)
APR 80 D T CHEN, V E NOBLE, S L SMITH
UNCLASSIFIED NRL-MR-4205 SBIE-AD-E000 418 NL

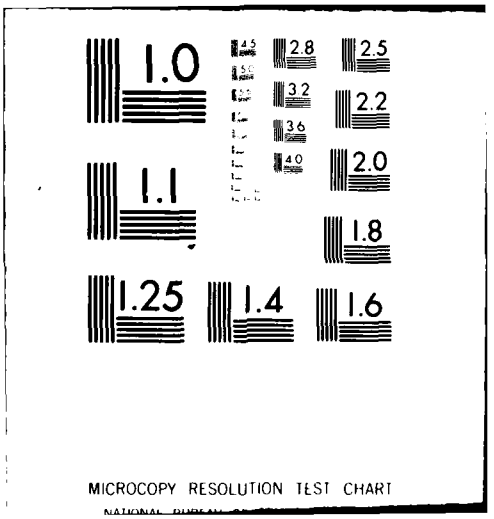
1.0
2.8
2.5
3.2
2.2
3.6
4.0
2.0
1.1
1.8
1.25
1.4
1.6
MICROCOPY RESOLUTION TEST CHART

NRL Memorandum Report 4205

On the Measurement of Geostrophic Ocean Currents by (NADIR) Satellite Altimeter

D. T. CHEN AND V. E. NOBLE

Space Sensing Applications
Space Science Division

AND

S. L. SMITH, III

Naval Surface Weapons Center
Dahlgren, Virginia

April 10, 1980

NAVAL RESEARCH LABORATORY
Washington, D.C.

SECURITY CLASSIFICATION OF THIS PAGE (When Data Entered)

REPORT DOCUMENTATION PAGE		READ INSTRUCTIONS BEFORE COMPLETING FORM
1. REPORT NUMBER NRL Memorandum Report 4205	2. GOVT ACCESSION NO. AD-A084986	3. RECIPIENT'S CATALOG NUMBER
4. TITLE (and Subtitle) ON THE MEASUREMENT OF GEOSTROPHIC OCEAN CURRENTS BY (NADIR) SATELLITE ALTIMETER		5. TYPE OF REPORT & PERIOD COVERED Final report on one phase of an NRL problem. 6. PERFORMING ORG. REPORT NUMBER
7. AUTHOR(s) D. T. Chen, S. L. Smith, III*, and V. E. Noble		8. CONTRACT OR GRANT NUMBER(s)
9. PERFORMING ORGANIZATION NAME AND ADDRESS Naval Research Laboratory Washington, D.C. 20375		10. PROGRAM ELEMENT, PROJECT, TASK AREA & WORK UNIT NUMBERS 63207N; 71-0932-0-0
11. CONTROLLING OFFICE NAME AND ADDRESS Naval Air Systems Command Code AIR 370C Washington, D.C. 20361		12. REPORT DATE April 10, 1980 13. NUMBER OF PAGES 31
14. MONITORING AGENCY NAME & ADDRESS(if different from Controlling Office)		15. SECURITY CLASS. (of this report) UNCLASSIFIED 15a. DECLASSIFICATION/DOWNGRADING SCHEDULE

16. DISTRIBUTION STATEMENT (of this Report)

Approved for public release; distribution unlimited.

17. DISTRIBUTION STATEMENT (of the abstract entered in Block 20, if different from Report)

18. SUPPLEMENTARY NOTES

*present address: Naval Surface Weapons Center, Dahlgren Laboratories, Dahlgren, VA.

19. KEY WORDS (Continue on reverse side if necessary and identify by block number)

Single-beam, pulse-limited nadir-looking satellite radar altimeter
Geostrophic ocean current
Orbit inclinations
Crossing pairs
Root-mean square noise
National Oceanic Satellite System
Multibeam altimeter

20. ABSTRACT (Continue on reverse side if necessary and identify by block number)

With the assumptions of accurately known marine geoid, satellite orbit, ionospheric and atmospheric propagation corrections, altimeter range precision, and dynamic components of sea-level deviations due to tides, barometric pressure, wind set-up, and storm surges, orbit inclination of 108° is shown to be the best choice among the three selected orbit inclinations (93°, 98°, and 108°) for the detection of geostrophic current vectors above 20° latitude. The second choice is 98° orbit inclination. The relationship shown as

$$V_R = CV$$

(Continues)

DD FORM 1 JAN 73 1473 EDITION OF 1 NOV 65 IS OBSOLETE
S/N 0102-014-6601

SECURITY CLASSIFICATION OF THIS PAGE (When Data Entered)

20. Abstract (Continued)

where V_R is the true local geostrophic current speed, V is the geostrophic current speed evaluated with the Root-Mean-Square (RMS) altimeter range noise, and C is a coefficient, can be used to derive V_R with the known C and V. The distribution of C and its lower and upper bounds can be calculated with the necessary ground truth programs. The RMS altimeter range noise, also, tends to bend the direction of the geostrophic current toward the east-west direction. In other words, the uncertainty in geostrophic current velocity determination is a function of the altimeter along-track slope measurement precision. Altimeter slope measurement uncertainty must be less than 0.1 $\widehat{\text{sec}}$ to achieve a minimum uncertainty in geostrophic current speed determination of 5 cm/sec, a goal set for the National Oceanic Satellite System (NOSS).

CONTENTS

ON THE MEASUREMENT OF GEOSTROPHIC OCEAN CURRENTS BY (NADIR) SATELLITE ALTIMETRY

1.0 INTRODUCTION

The following discussion considers the problem of measuring geostrophic ocean current velocities with a single-beam, pulse-limited, nadir-looking satellite radar altimeter similar to those on SKYLAB, GEOS, and SEASAT. It is assumed that sufficient information is available to accurately determine the instantaneous, local, dynamic ocean heights as measured with respect to the marine geoid. These measurements require precise knowledge of the local geoid, satellite orbit, and non-current-related factors affecting measurement of ocean surface topography. It is also further assumed that the differences in satellite orbit slope errors at orbit crossings are negligible in their effects on the derivation of the local dynamic ocean surface slopes.

Principal altimeter measurement corrections include uncertainties of the order of 20 cm for both atmospheric propagation and ionospheric effects [Saastamoinen, 1971; Davies, 1965; Thomason, et al, 1979]. Dynamic processes causing local deviations of the ocean surface topography from the marine geoid include: tides (30 cm open-ocean, 15 m coastal) [Neumann and Pierson, 1966; Doodson, 1958; Stoker, 1957]; barometric pressure gradients (up to 1 m); wind set-up and storm surges (up to 10 m in coastal regions) [Neumann and Pierson, 1966]; and density gradients associated with current systems (1 m associated with strong boundary currents such as the Gulf Stream and the Kuroshio Current) [Stommel, 1966; Stommel and Yoshida, 1972]. The measurement problem is illustrated in Figure 1.1.

Manuscript submitted February 26, 1980.

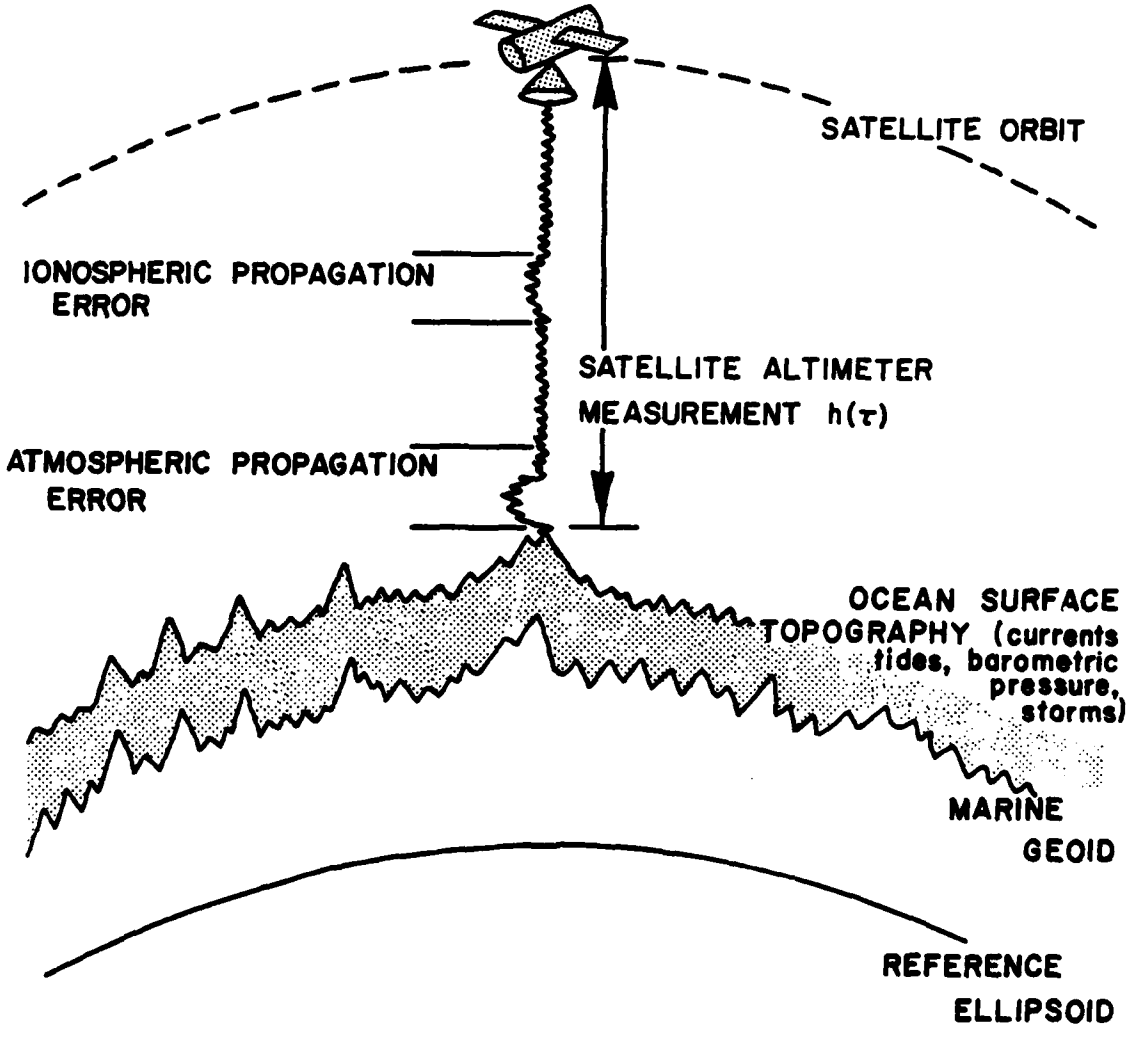

Fig. 1.1 - Configuration of altimeter measurement

2.0 MEASUREMENTS/ASSUMPTIONS

2.1 Assumptions. For the following discussions it is assumed that:

(1) The marine geoid is accurately known.

(2) The satellite orbit is accurately determined.

(3) Data are available for accurate determination of ionospheric and atmospheric propagation corrections to satellite altimeter range measurements.

(4) Satellite radar altimeter range measurement precision has been determined.

(5) Dynamic components of sea-level deviations due to tides, barometric pressure, wind set-up, and storm surges are accurately determined from models and other data input.

2.2 Measurements. For the following discussions, it is presumed that the assumptions above are satisfied and that the measurement to be considered is the current-related dynamic ocean surface topography within the precision limit of the radar altimeter measurement. Using time (t) as the parameter to define position along the sub-satellite track, the current-related dynamic ocean surface topography can be expressed as:

$$D(t) = O(t) - [h(t)-\varepsilon_I(t)-\varepsilon_A(t)]- [G(t)+T(t)+B(t)+W(t)] \qquad (2.1)$$

where:

$O(t)$ is the satellite orbit,

$h(t)$ is the radar range measurement,

$\varepsilon_I(t)$ is the ionospheric propagation correction,

$\varepsilon_A(t)$ is the atmospheric propagation correction,

$G(t)$ is the marine geoid,

$T(t)$ is the tide,

$B(t)$ is the topographic variation due to barometric pressure, and

$W(t)$ is the topographic variation due to wind set-up and storm surges.

Both O(t) and G(t) are defined with respect to the center of mass of Earth. The determinations of: O(t), $\varepsilon_I(t)$, $\varepsilon_A(t)$, G(t), T(t), B(t), and W(t) are assumed to be absolutely correct.

3.0 DETERMINATION OF GEOSTROPHIC OCEAN CURRENT

Following Sverdrup, et al. [1946] ocean currents may be divided into three groups: (1) currents that are related to the distribution of density in the sea (barotropic and baroclinic geostrophic currents), (2) currents that are caused directly by the stress that the wind exerts on the sea surface (wind driven currents), and (3) tidal currents and currents associated with internal waves. In accordance with the above-stated assumptions, the following discussion concerns only the geostrophic (density-gradient) currents.

The geostrophic current is determined by a balance between the Coriolis force (acceleration due to the earth's rotation and the pressure gradients (slope of the isobaric surfaces) in the ocean. The numerical value of the ocean-current velocity for a given slope of an isobaric surface is given by:

$$V_R(\phi) = g \frac{\tan S_R}{2\omega \sin\phi} \tag{3.1}$$

where:

$V_R(\phi)$ = geostrophic current speed in m/sec at Latitude ϕ,
g = acceleration of gravity,
$\tan S_R$ = slope of the isobaric surface,
S_R = angle of the dynamic ocean surface to the local horizontal plane,
ω = angular velocity of rotation of earth, and
ϕ = geographic latitude which is positive and negative for northern and southern hemispheres, respectively.

In the northern hemisphere ($\phi>0$), the current direction is 90° to the left of the direction of positive slope. In the sourthern hemisphere ($\phi<0$), the current direction is to the right.

Taking: $g = 9.80$ m/sec^2, and $\omega = 7.27 \times 10^{-5}$ rad/sec in Equation (3.1)

$$V_R(\phi) = 6.74 \times 10^4 \frac{\tan S_R}{\sin\phi} \tag{3.2}$$

At 45° latitude, for example:

$$V_R(45°) = 9.53 \times 10^4 \tan S_R \tag{3.2a}$$

and if $\tan S_R = 10^{-5}$ (10 cm height difference over 10 km):

$$V_R(45°) \simeq 1 \text{ m/sec} \simeq 2 \text{ kts.} \tag{3.2b}$$

If the surface slope is expressed in dimensions of $\widehat{\text{sec}}$, the expression for geostrophic current speed becomes, with $\omega = 15$ $\widehat{\text{sec}}$/sec,

$$V_R(\phi) = 0.3268 \tan S_R / \sin\phi \tag{3.3}$$

at 45° latitude, for example,

$$V_R(45°) = 0.462 \tan S_R \tag{3.3a}$$

and if $\tan S_R = 1$ $\widehat{\text{sec}}$

$$V_R(45°) \simeq 0.5 \text{ m/sec} \simeq 1 \text{ kt.} \tag{3.3b}$$

4.0 GEOSTROPHIC CURRENT INFERRED FROM ALTIMETER MEASUREMENTS AT THE CROSSING POINT

It is well recognized that a single-beam nadir radar altimeter cannot provide measurement of the geostrophic current vector from a single along-track surface slope. The current derived from a single along-track surface slope is, at best, the across-track current component, let alone the true geostrophic current. The scheme discussed in Section 6.0 gives reasonable recourse for short term descriptions of the geostrophic current system.

Nevertheless, the true local geostrophic current velocities can be inferred from altimeter measurements at the satellite subtrack crossing points with the additional assumption: the geostrophic

current system has not experienced significant changes during the time interval which is required for the satellite to complete these crossings. In the case of SEASAT-A, it takes the satellite less than 11 hours to complete a crossing pair [Cutting, et al, 1977]. Since most of the time scales for geostrophic phenomena in the ocean are longer than 11 hours, the assumption is valid, most of the time. From the two local dynamic ocean surface slopes derived from the altimeter measurements made at the crossings the local dynamic ocean surface plane can be constructed from which its true slope vector can be evaluated for this local plane [Sokolnikoff,1951]. Then the geostrophic current velocities may be determined from Equation (3.1) with the known directions.

Let $\overrightarrow{OA}_1$ and $\overrightarrow{OA}_2$ be these two slope vectors without separation at origin O in a Right Hand Rectangular Cartesian Coordinates as shown in Figure 4.1 where

$$A_1 = (t_1 \cos(\pi - \psi/2),\ t_1 \sin(\pi - \psi/2),\ t_1 s_1).$$

$$A_2 = (t_2 \cos(\pi + \psi/2),\ t_2 \sin(\pi + \psi/2),\ t_2 s_2),$$

and t_i and s_i are the along-track horizontal distance and measured slope, respectively. The intersection angle ψ between the ascending and the descending orbits is bisected by the x-axis which is, of course, in the local east-west direction. These intersection angles with respect to latitude for selected orbit inclinations are shown in Figure 4.2.

The plane which contains points A_1, A_2, and the origin O has the general form of

$$a_o x + b_o y + c_o z + d_o = 0 \qquad (4.1)$$

with the origin O in the plane $d_o = 0$ or

$$z = ax + by \qquad (4.2)$$

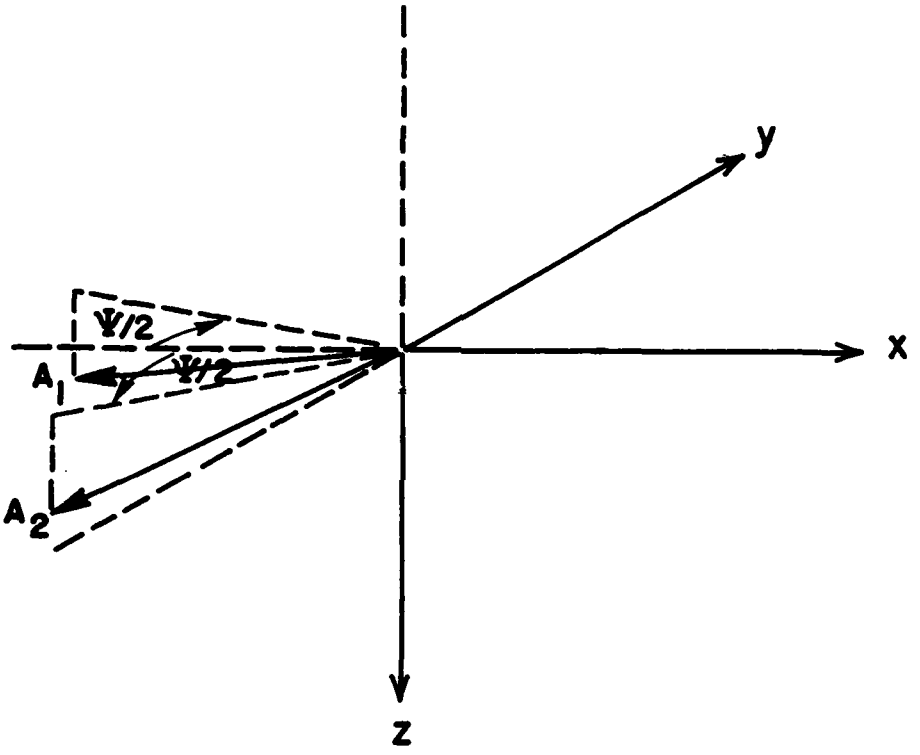

Fig. 4.1 - Rectangular Cartesian coordinates with Jacobian = 1

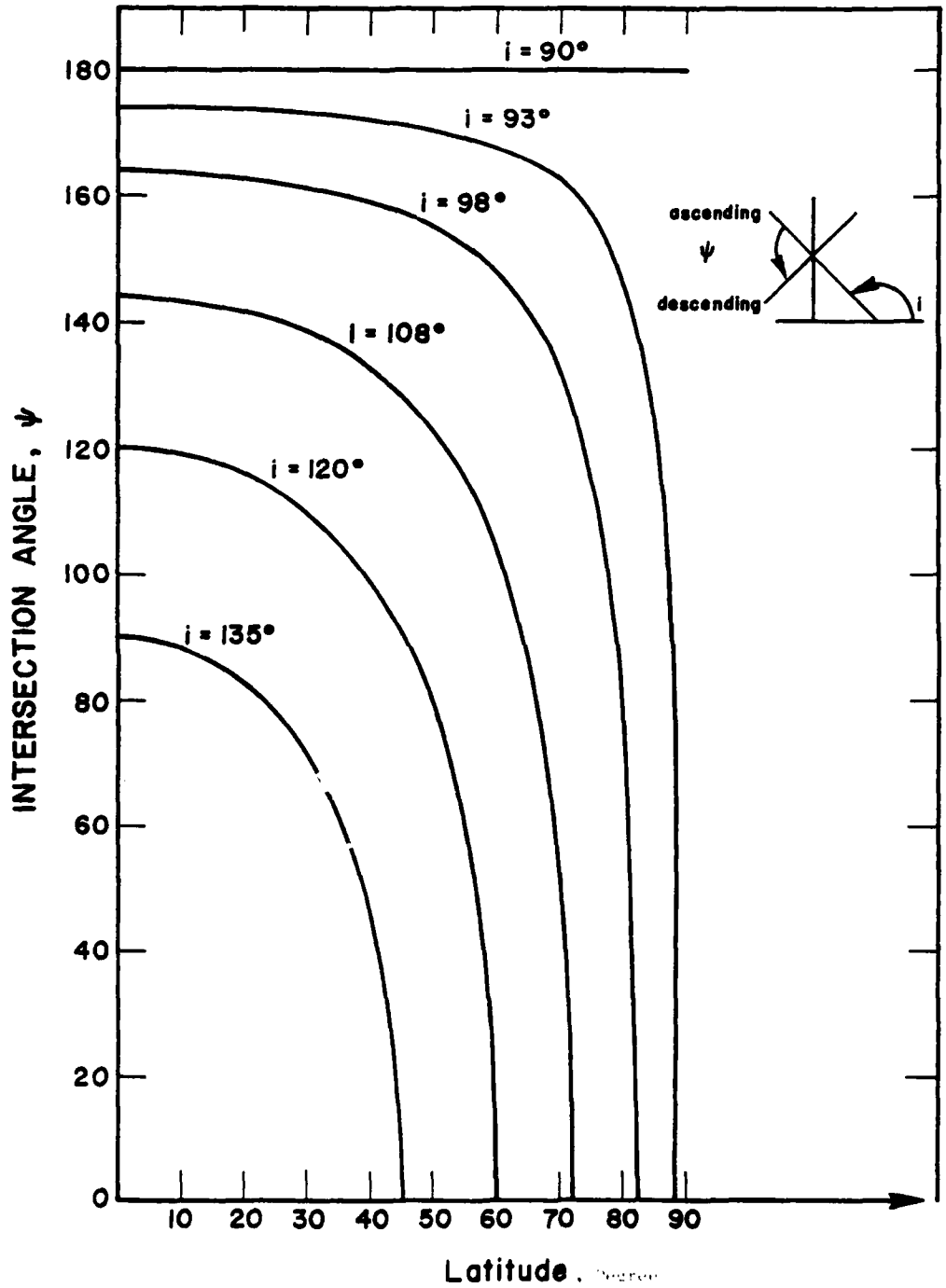

Fig. 4.2 - Intersection angle with respect to latitude for orbit inclinations of 90°, 93°, 98°, 108°, 120° and 135°

Substituting the coordinates of points A_1 and A_2 into Equation (4.2)

$$\cos(\psi/2)\ a - \sin(\psi/2)\ b = -\ s_1 \tag{4.3}$$

$$\cos(\psi/2)\ a + \sin(\psi/2)\ b = -\ s_2 \tag{4.4}$$

Therefore, from Equations (4.3) and (4.4)

$$a = -\frac{s_1 + s_2}{2\sin(\psi/2)} \tag{4.5}$$

$$b = \frac{s_1 - s_2}{2\sin(\psi/2)} \tag{4.6}$$

With a and b known, Equations (4.2), the plane which contains points A_1, A_2, and the origin 0 is

$$\frac{s_1 + s_2}{2\cos(\psi/2)}\ x - \frac{s_1 - s_2}{2\sin(\psi/2)}\ y + z = 0 \tag{4.7}$$

The direction cosines of the normal to this plane are

$$\frac{s_1 + s_2}{2\cos(\psi/2)}\ ,\ -\frac{s_1 - s_2}{2\sin(\psi/2)}\ ,\ 1 \tag{4.8}$$

and the angle, γ_n, of the normal to the z-axis is defined as

$$\cos\gamma_n = \left\{\left[\frac{s_1 + s_2}{2\cos(\psi/2)}\right]^2 + \left[\frac{s_1 - s_2}{2\sin(\psi/2}\right]^2 + 1\right\}^{-1/2} \tag{4.9}$$

for acute angle. Since Equation (4.7) represents a plane, the normal line defined by (4.8) can be a family of lines. Let the particular normal line be chosen to be such that it intersects z-axis. The line which is perpendicular to this normal line and yet passes through the origin lies in the plane defined by Equation (4.7) and, from Equation (4.9)

$$\sin\gamma_t = \cos\gamma_n = \left\{\left[\frac{s_1 + s_2}{2\cos(\psi/2)}\right]^2 + \left[\frac{s_1 - s_2}{2\sin(\psi/2)}\right]^2 + 1\right\}^{-1/2}$$

where γ_t is the angle between this line and the z-axis. The slope

$(\tan S_R)$ of this line to the xy plane can, thus, be calculated as

$$\tan S_R = \tan\gamma_n = \left\{ \left[\frac{s_1 + s_2}{2\cos(\psi/2)}\right]^2 + \left[\frac{s_1 - s_2}{2\sin(\psi/2)}\right]^2 \right\}^{1/2}$$

$$= (s_1^2 + s_2^2 - 2s_1 s_2 \cos\psi)^{1/2}/\sin\psi \qquad (4.10)$$

for acute angle. The equation for this normal line, from Expression (4.8), is

$$\frac{x - x_o}{\left[\frac{s_1 + s_2}{2\cos(\psi/2)}\right]} = \frac{y - y_o}{-\left[\frac{s_1 - s_2}{2\sin(\psi/2)}\right]} = z - z_o$$

For $(x_o, y_o, z_o) = (0, 0, z_o)$ which is a point on the z-axis,

$$\frac{-x}{\left[\frac{s_1 + s_2}{2\cos(\psi/2)}\right]} = \frac{y}{-\left[\frac{s_1 - s_2}{2\sin(\psi/2)}\right]} = z - z_o \qquad (4.11)$$

Equation (4.11) can be written also as

$$\left[\frac{s_1 - s_2}{2\sin(\psi/2)}\right]x + \left[\frac{s_1 + s_2}{2\cos(\psi/2)}\right] y = 0 \qquad (4.12)$$

$$x - \left[\frac{s_1 + s_2}{2\cos(\psi/2)}\right] (z - z_o) = 0 \qquad (4.13)$$

$$y + \left[\frac{s_1 - s_2}{2\sin(\psi/2)}\right] (z - z_o) = 0 \qquad (4.14)$$

Equation (4.12) is, indeed, the direction of the line on the xy-plane which is perpendicular to Equation (4.11) and has a slope shown by Equation (4.10) with the xy-plane. Therefore, from Equation (4.12),

$$y = \left[\frac{s_2 - s_1}{s_2 + s_1} \cot(\psi/2)\right] x$$

or the angle θ with the x-axis is

$$\tan\theta = \frac{s_2 - s_1}{s_2 + s_1} \cot(\psi/2) \tag{4.15}$$

The whole mathematical scheme so far can be categorized as:

(1) $\overrightarrow{OA}_1$ represents the slope vector for the ascending orbit which intersects decending orbit at an intersecting ground angle of ψ. The decending orbit has the slope vector $\overrightarrow{OA}_2$. The reference system is the local Rectangular Cartesian Coordinates with x-axis in East, y-axis in North and z-axis in the direction of the local gravity. There is no separation between $\overrightarrow{OA}_1$ and $\overrightarrow{OA}_2$ at the origin O.

(2) Equation (4.7) represents the plane which contains the slope vectors $\overrightarrow{OA}_1$ and $\overrightarrow{OA}_2$.

(3) The true local slope vector of the plane represented by Equation (4.7) has the magnitude tanS, represented by Equation (4.10), and has the true directional angle θ with the x-axis as represented by Equation (4.15). This angle θ has 180° ambiguity. Nevertheless it should not be difficult to figure out the correct one.

It is essential, and, also, important to evaluate the effects of the noises in the measurements of s_1 and s_2 on Equations (4.10) and (4.15). Let

$$s_1 = S_1 + 2\Delta S_1 \tag{4.16}$$

$$s_2 = S_2 + 2\Delta S_2 \tag{4.17}$$

where S_1 and S_2 are the desired measurements and ΔS_1 and ΔS_2 are the noises associated with the measurements of S_1 and S_2, respectively. The factor 2 is for the worst case which indicates the same noise at the origin with opposite sign. In space application it will be further assumed that the noise levels on the measurements on each track are the same, i.e.,

$$\Delta S_1 = \Delta S_2 = \Delta S \tag{4.18}$$

This is not generally true, but serves to bound the problem.

And in Equation (4.18), ΔS is the Root-Mean-Square (RMS) noise in the measurement. Therefore, Equations (4.16) and (4.17) are

$$S_1 = S_1 + 2\Delta S \tag{4.19}$$

$$S_2 = S_2 + 2\Delta S \tag{4.20}$$

Henceforth, from Equations (4.10), (4.19) and (4.20)

$$\tan S = [(S_1 + 2\Delta S)^2 + (S_2 + 2\Delta S)^2 - 2(S_1 + 2\Delta S) \cdot (S_2 + 2\Delta S) \cos\psi]^{1/2} / \sin\psi \tag{4.21}$$

and, from Equation (4.15), (4.19) and (4.20)

$$\tan\theta = \frac{S_2 - S_1}{S_2 + S_1 + 4\Delta S} \cot\psi \tag{4.22}$$

In general, S_1 and S_2 do not equal to each other. And, furthermore, $S_1 \neq 2\Delta S$ and $S_2 \neq 2\Delta S$, Equations (4.21) and (4.22) appear to be highly nonlinear and should be treated accordingly for the effects of ΔS on S and θ. Nevertheless, after regrouping

$$\tan S = [\tan^2 S_R + \tan^2 \Delta S_\varepsilon + \tan^2 \Delta S_\varepsilon' - (S_1 + S_2 - 2\Delta S)^2 / \sin^2 \psi]^{1/2} \tag{4.23}$$

and

$$\tan\theta = [1 - F(S_1, S_2, \Delta S)] \tan\theta_R \tag{4.24}$$

where

$$\tan S_R = \frac{[S_1^2 + S_2^2 - 2S_1 S_2 \cos\psi]^{1/2}}{\sin\psi} \tag{4.25}$$

$$\tan \Delta S_\varepsilon = \frac{[2(2\Delta S)^2 - 2(2\Delta S)^2 \cos\psi]^{1/2}}{\sin\psi} , \tag{4.26}$$

$$\tan\Delta S_\varepsilon' = \frac{[(2\Delta S)^2 + (S_1 + S_2)^2 - 2(2\Delta S)(S_1 + S_2)\cos\psi]^{1/2}}{\sin\psi} , \tag{4.27}$$

$$\tan\theta_R = \frac{S_2 - S_1}{S_2 + S_1} \cot\psi , \tag{4.28}$$

and

$$F(S_1, S_2, \Delta S) = \frac{2(2\Delta S)}{S_2 + S_1 + 2(2\Delta S)} . \tag{4.29}$$

The terms $\tan S_R$ and $\tan\theta_R$ are the desired terms without the effects of the measurement noise. The terms $\tan\Delta S_\varepsilon$, $\tan\Delta S_\varepsilon'$, and $F(S_1, S_2, \Delta S)$ are all introduced by non-zero ΔS.

In view of the nonlinear characters in terms of S_1, S_2, and ΔS in Equations (4.23) and (4.24) for S and θ it is desirable to set S_1 and S_2 to zero in order to demonstrate the different effects on S and θ due to the same ΔS with various orbit inclinations. Thus, Equations (4.25), (4.26), (4.27), (4.28), and (4.29) are reduced to

$$\tan S_R = 0 , \tag{4.30}$$

$$\tan\Delta S_\varepsilon = \frac{2\sqrt{2}\ \Delta S\ (1 - \cos\psi)^{1/2}}{\sin\psi} , \tag{4.31}$$

$$\tan\Delta S_\varepsilon' = \frac{2\Delta S}{\sin\psi} , \tag{4.32}$$

$$\tan\theta_R = 0 , \tag{4.33}$$

and

$$F(0, 0, \Delta S) = 1 \tag{4.34}$$

Therefore Equations (4.23) and (4.24) become

$$\tan S = \tan\Delta S_\varepsilon = \frac{2\sqrt{2}\ \Delta S\ (1 - \cos\psi)^{1/2}}{\sin\psi}$$

$$= 2\Delta S \sec(\psi/2) \quad , \tag{4.35}$$

and

$$\tan\theta = \tan\theta_R = 0 \tag{4.36}$$

Equations (4.35) and (4.36) show that the local slope generated by ΔS alone is in either the east or the west direction. The conclusions presented by Equations (4.35) and (4.36) are quite obvious and should be used to ascertain the validities of Equations (4.23) and (4.24).

Nevertheless, in a typical Western North Atlantic Ocean, let $S_1 = -1\ \widehat{\sec}$ and $S_2 = -9/10\ \widehat{\sec}$ which give a Gulf-Stream-like current. Let the root-mean-square noise be $1\ \widehat{\sec}$, i.e., 2.5 cm root-mean-square altimeter precision with measurements separated by 10 km [ref. Figure 5.1, Equations (4.16) and (4.17)]. By using Equations (3.1), (4.23), (4.24), (4.25), (4.26), (4.27), (4.28) and (4.29), for the worst possible case where ΔS assumes the same sign as those of S_1 and S_2 Table 4.1 can be computed for orbit inclinations 93°, 98° and 108° where

ψ = crossing angle between ascending and descending orbits as defined in Figure 4.1 and given in Figure 4.2,

V_R = the real geostrophic current speed in m/sec,

V = The geostrophic current speed in m/sec computed with the non-zero root-mean-square noise,

δ_R = the real direction of geostrophic current with respect to the local east in a counter clockwise direction, and

δ = the direction derived for the geostrophic current V in the same sense of direction as defined for δ_R.

Figure 4.3 shows the plots of V_R and V with respect to the latitude for orbit inclinations of 93°, 98°, and 108° while Figure 4.4 shows the plots of δ_R and δ for these V_R and V. The broken lines in Figures 4.3 and 4.4 represent V and δ, respectively, which are computed with the Root-Mean-Square (RMS) noise ΔS, and the solid lines represent V_R and δ_R, respectively, which are, of course, computed without the RMS noise.

V_R, V, δ_R, and δ computed with $S_1 = -1\widehat{\text{sec}}$, $S_2 = -0.9\widehat{\text{sec}}$, and $\Delta S = 1\widehat{\text{sec}}$ for 93°, 98°, and 108° Orbit Inclinations

Orbit Inclination \ Latitude		0	10	20	30	40	50	60	70	80
93°	ψ	174	173.9	173.62	173.08	172.16	170.66	167.98	162.4	144.92
	tan S_R	17.787	17.447	16.661	15.408	13.589	11.397	8.858	6.064	3.079
	tan S	55.796	54.729	52.264	48.332	42.624	35.748	27.779	19.011	9.634
	θ_R	26.61	26.20	25.22	23.46	20.91	17.74	13.87	9.43	4.29
	θ	9.15	8.98	8.64	7.97	7.01	5.88	4.57	3.03	1.37
	V_R	-	32.835	15.920	10.071	6.909	4.862	3.343	2.109	1.022
	V	-	102.998	49.938	31.590	21.670	15.250	10.483	7.174	3.197
	δ_R	-	116.2	115.22	113.46	110.91	107.74	103.87	99.43	94.29
	δ	-	98.98	98.64	97.97	97.01	95.88	94.57	93.03	91.37
98°	ψ	164	163.76	162.96	161.5	159.06	155	147.68	131.98	73.46
	tan S_R	6.648	6.552	6.255	5.770	5.106	4.28	3.333	2.290	1.211
	tan S	20.844	20.542	19.610	18.088	16.004	13.409	10.431	7.144	3.626
	θ_R	10.43	10.26	9.76	8.92	7.86	6.45	4.74	2.69	-0.92
	θ	3.38	3.32	3.15	2.92	2.52	2.06	1.55	0.86	-0.29
	V_R	-	12.33	5.98	3.77	2.60	1.83	1.26	0.80	0.40
	V	-	38.65	18.73	11.82	8.14	5.72	3.94	2.48	1.20
	δ_R	-	100.26	99.76	98.92	97.86	96.45	94.74	92.69	89.08
	δ	-	93.32	93.15	92.92	92.52	92.06	91.55	90.86	89.71
108°	ψ	144	143.42	141.6	138.18	132.42	122.54	103.66	50.76	
	tan S_R	3.004	2.595	2.826	2.604	2.309	1.943	1.523	1.143	
	tan S	9.398	9.256	8.837	8.137	7.205	6.045	4.701	3.219	
	θ_R	4.12	4.06	3.78	3.38	2.75	1.95	0.74	-2.46	
	θ	1.32	1.32	1.20	1.09	0.86	0.63	0.23	-0.79	
	V_R	-	5.57	2.70	1.70	1.17	0.83	0.57	0.40	
	V	-	17.42	8.44	5.32	3.66	2.58	1.77	1.12	
	δ_R	-	94.06	93.78	93.38	92.75	91.95	90.74	87.54	
	δ	-	91.32	91.20	91.09	90.86	90.63	90.23	89.21	

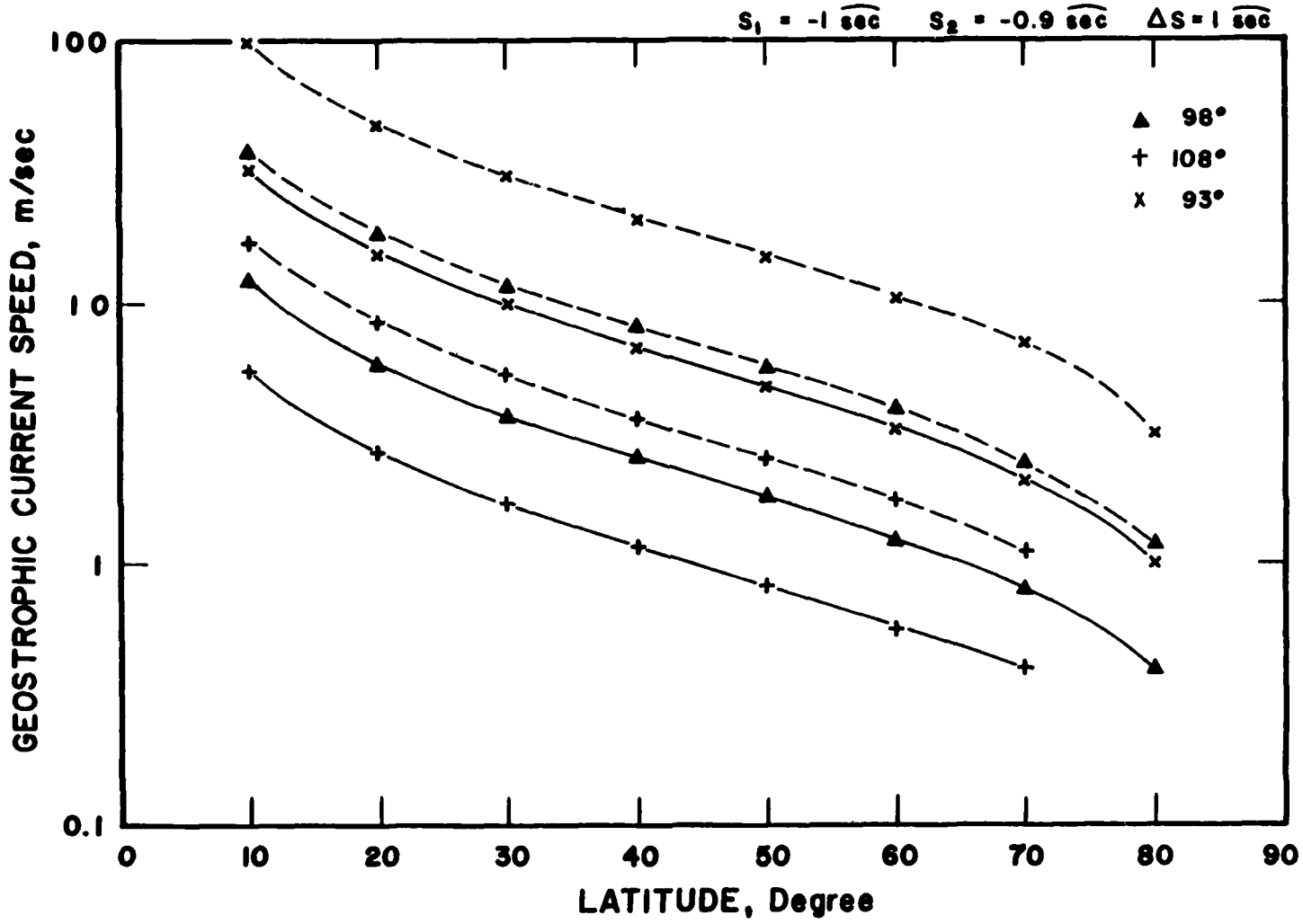

Fig. 4.3 Geostrophic currents inferred w/ (dashed curves) and w/o (solid curves) RMS noise for 93°, 98°, and 108° orbit inclinations

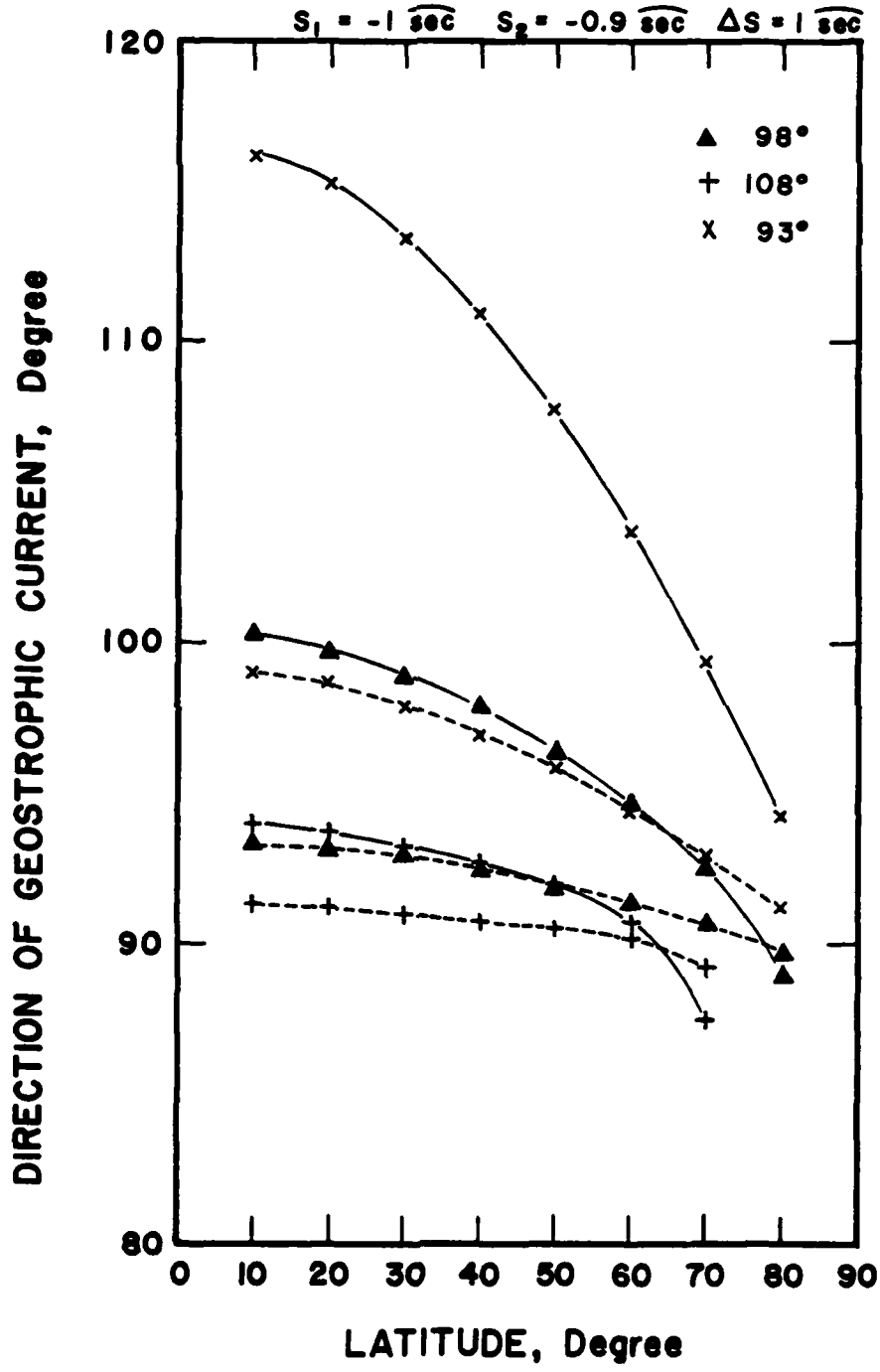

Fig. 4.4 - Geostrophic current direction wrt the east w/ (dashed curves) and w/o (solid curves) RMS noise for 93°, 98°, and 180° orbit inclinations

However, several observations can be made regarding Figures 4.3 and 4.4. (1) There are nearly constant relationships resulting from the assumptions such as

$$V_R = C\ V \tag{4.37}$$

that can be made between each pair of V_R and V for various orbit inclinations. In reality, the value of ΔS is Gaussian-distributed, and a range of C in Equation (4.37) should be evaluated, for each orbit inclination, and independently verified by selective ground truth programs. Nevertheless orbit inclination 108° does have the smallest magnitude for C among the inclinations selected. (2) The effects due to RMS noise on δ_R appear to bend δ_R toward local north or south in direction as predicted by Equation (4.36). (3) The orbit inclination 108° shows to be the best among the three orbit inclinations in the determination of reasonable V_R and δ_R. Therefore, this orbit inclination is the best for geostrophic current determination for the choices selected.

5.0 UNCERTAINTY IN SATELLITE ALTIMETER MEASUREMENT OF OCEAN SURFACE SLOPE

A slope of 10^{-5} (10 cm height difference in 10 km) is approximately equal to an angular slope of $2\overset{\frown}{\text{sec.}}$ If all of the assumptions of Section 2.1 are satisfied, the uncertainty of the altimeter along-track slope determination is limited by the measurement precision.

Conservative expressions for along-track slope measurement uncertainties are shown in Figure 5.1 for the cases of 5 cm RMS and 10 cm RMS altimeter noise ΔS. The RMS slope uncertainty is expressed in dimensions of $\overset{\frown}{\text{sec.}}$ In the estimation, if the RMS noise is 5 cm, and the measurements are made at 2 points separated by 10 km, the RMS slope uncertainty is 10^{-5}, or $2\overset{\frown}{\text{sec,}}$ which is for the worst case estimation.

It has been demonstrated that proper filtering (weighted averaging) of the along-track radar altimeter data can greatly reduce the along-track slope measurement uncertainties. Uncertainties as low as $0.1\overset{\frown}{\text{sec}}$ have been obtained from SEASAT altimeter data (B. Chovitz and B. Douglas, National Oceanic Survey, NOAA, private communications). The averaging techniques define the space-scale of precise slope determinations.

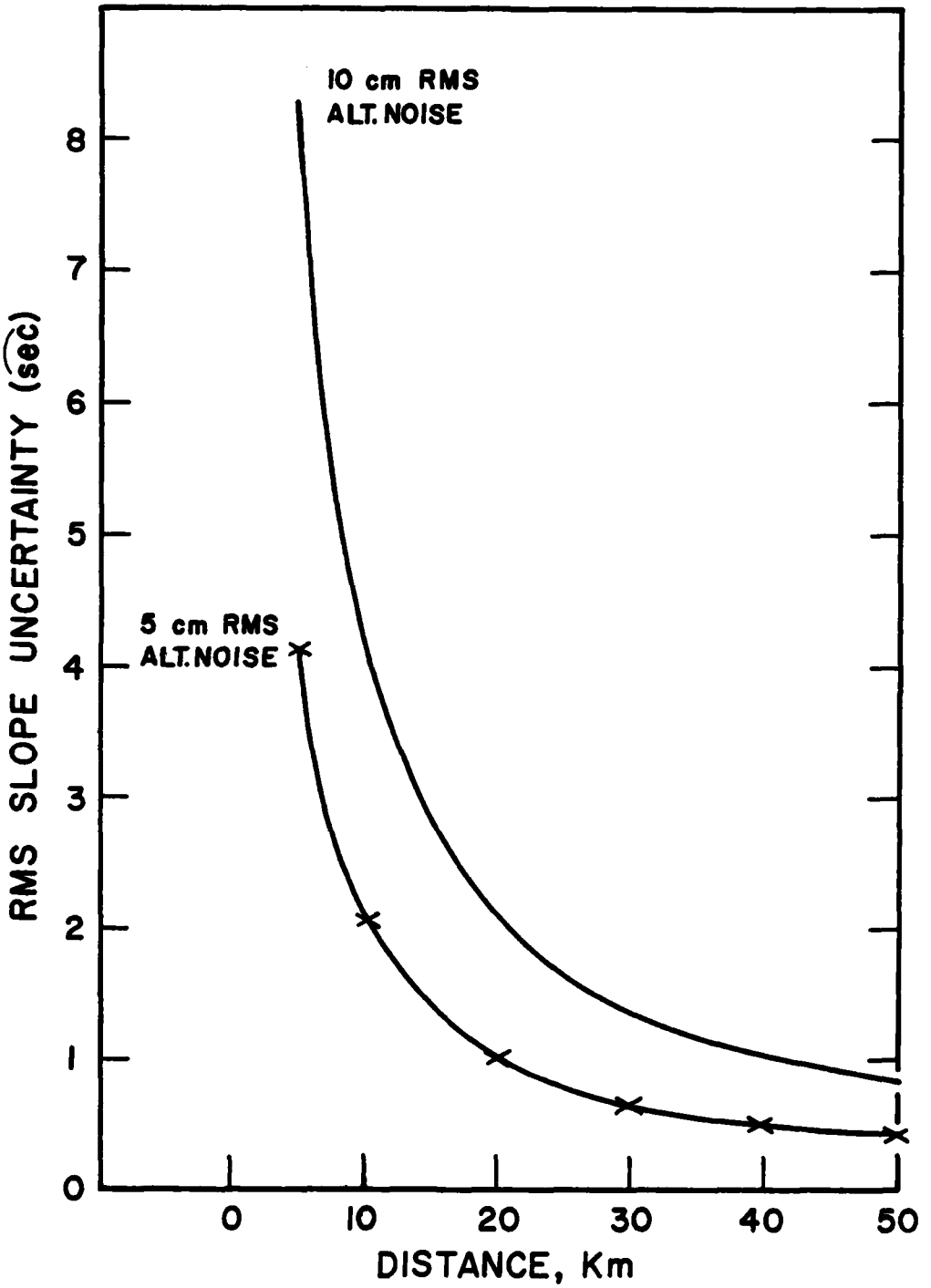

Fig. 5.1 - Along-track slope measurement uncertainties

Since the current-speed uncertainties are directly proportional to slope uncertainties, without elaborated discussions on the proper weighting techniques and the spatial scale factors, illustrative examples of current speed determinations are based upon the conservative expressions as shown in Figure 5.1 wherever they are appropriate.

The uncertainty of determination of the components of surface slope along-track may be expressed as a product of a latitude-inclination-direction-dependent Error Factor with the along-track slope uncertainty. The latitude-dependence of North and East slope error factors for selected orbit inclinations of 73°, 100°, 105°, and 110° are shown in Figure 5.2.

The slope component uncertainties as a function of latitude for an along-track slope uncertainty of $0.85\widehat{\sec}$ and an orbit inclination of 98° (approximately sun-synchronous) are shown in Figure 5.3. Under the conservative assumptions of Figure 5.1, a slope uncertainty of $0.85\widehat{\sec}$ implies a distance separation of 50 km for 10 cm RMS altimeter noise, or a distance separation of 25 km for 5 cm RMS altimeter noise.

6.0 DISCUSSION

From Figures 4.3 and 4.4 it is seen that: (1) The uncertainties in the determination of geostrophic current rapidly decrease in their magnitude and, yet, maintain the nearly constant relationship as given by Equation (4.37) for increasing values of latitude ϕ. Nevertheless, a range of values of C, in Equation (4.37), can be determined by ground truth for Gaussian-distributed RMS noise ΔS. For each orbit inclination the distribution of C and its lower and upper bounds for the values of C can be calculated. With the known C, ΔS, V, and δ, the true local geostrophic current parameters V_R and δ_R can be evaluated by Equation (4.37) with Figures 4.3 and 4.4. (2) The effects due to RMS noise on the determination of geostrophic current directions show the directional angle δ, with respect to the local east, to be more in local east-west oriented direction than that shown by the true directional

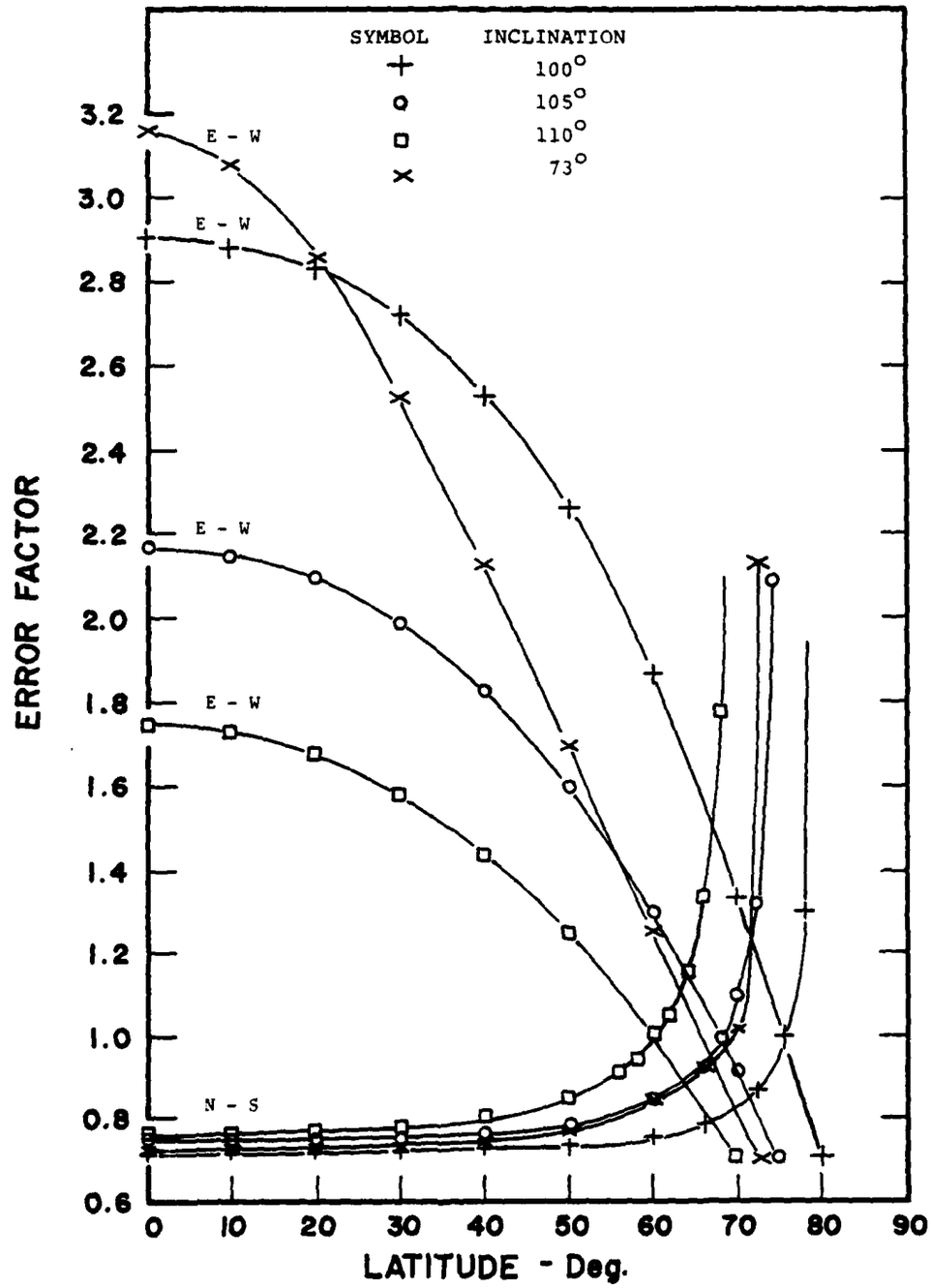

Fig. 5.2 - Error factors in N - S and E - W directions for different orbit inclinations

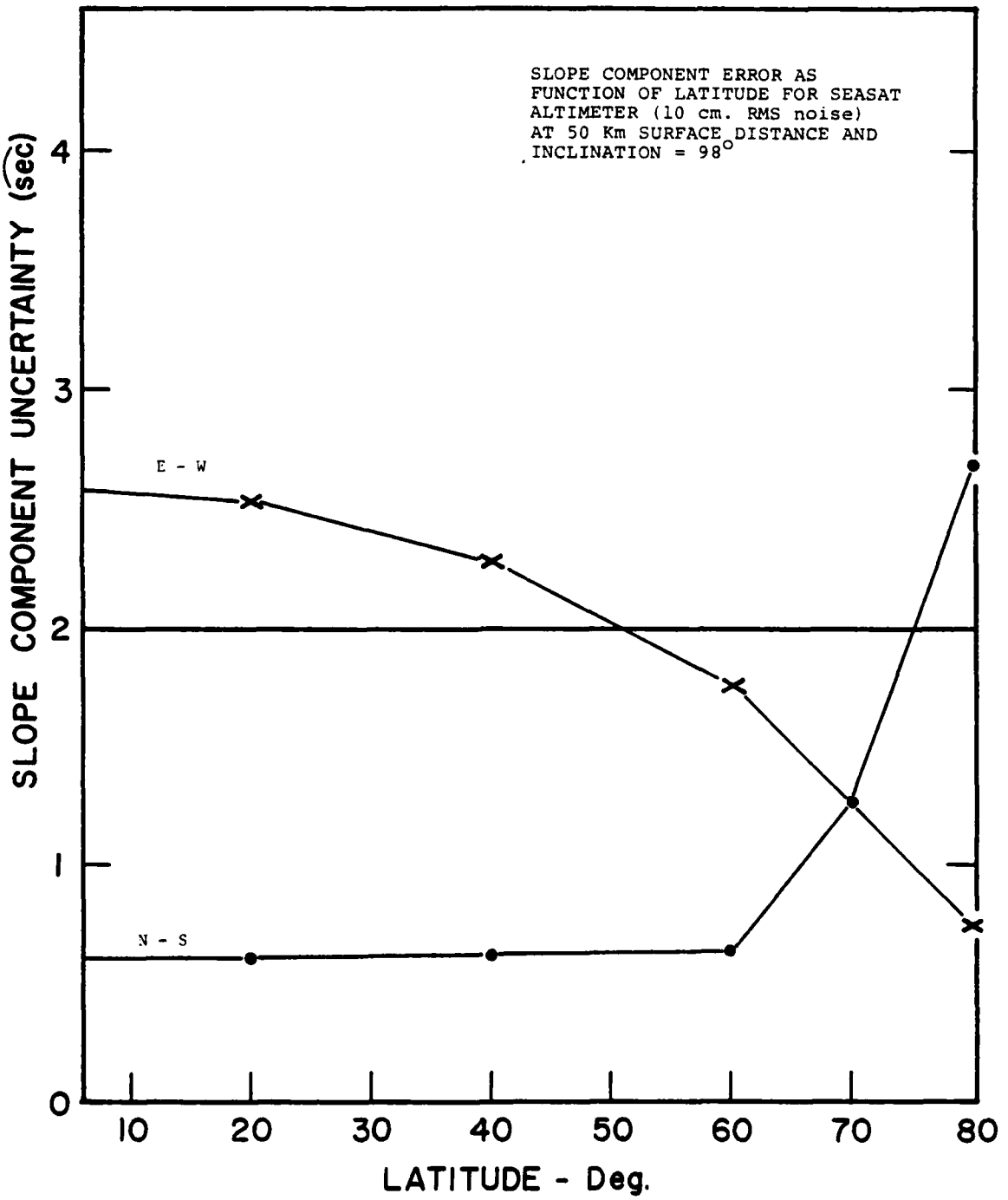

Fig. 5.3 - Along-track slope component uncertainties with 0.85 sec slope uncertainty for 98° orbit inclination

angle δ_R. (3) For $S_1 = -1\widehat{sec}$, $S_2 = -0.9\widehat{sec}$, and $\Delta S = 1\widehat{sec}$ the best orbit inclination, among the three studied for the detection of geostrophic current velocity, is 108°. The second choice appears to be 98°. (4) It is also important to point out that, with the assumptions made for the derivation for geostrophic current calculation, the results are meaningful only for latitude 20° and up.

As has been demonstrated from SEASAT-A analyses, an altimeter precision of 10 cm is adequate to detect and provide first-order speed estimates for Western Boundary currents (e.g. Gulf Stream, Kuroshio) which have characteristic speeds of the order 1 m/sec, and represent the higher portion of the range of current speeds to be measured. The precision goal for measurement of current speeds within the National Oceanic Satellite System (NOSS) is 5 cm/sec. From Figures 4.3 and 4.4 and Equations (3.3), (3.3a), and (3.3b), it is seen that altimeter surface measurement uncertainty must be of the order of $0.1\widehat{sec}$ to achieve the NOSS current speed measurement goal for 20° latitude and up.

The altimeter measurement requirement for $0.1\widehat{sec}$ precision is equivalent to a slope precision of 5×10^{-7} (5 cm in 100 km). This slope precision is necessary to determine the speed of such important features as the Southern Ocean Current and the Laborador Drift Current.

Since in reality, the assumptions made in Section 2.1 cannot be fully satisfied, the averaging and optimizing techniques such as those employed by Huang, et al (1978) should be used so that the effects due to the partial invalidities of some of the assumptions can be alleviated.

For high latitudes a network of in-situ current measurements used by Wunsch (1977) can certainly be used to reduce the uncertainties in the altimeter-derived current measurements. These uncertainties are primarily, caused by the small crossing angles and the lack of information on the north component of the slopes at the high latitudes. The main purpose of the in-situ current measurement is to provide the boundary condition for the current system.

A multi-beam altimeter (McGoogan and Walsh, 1978) can provide several off-nadir measurements simultanteously. The deployment of this type of instrument along-track as well as across-track in space will have several advantages:

(1) The true local ocean surface slope vectors can be obtained for the individual track without waiting for crossings to occur. Henceforth, the true local geostrophic ocean current velocities, not only the components across-track, can be inferred from a single pass.

(2) The effects due to orbit altitude rate uncertainties on the ocean surface slope measurements are greatly reduced in comparison to those provided by the single-beam nadir altimeter.

(3) The resolution of both across-track and along-track measurements can be changed if desired.

Further airborne tests and analyses of this multi-beam instrument are required to be pursued in order to answer some of the questions associated, always, with new instruments.

7.0 CONCLUSION

Orbit inclination of 108° is the best choice among the three selected orbit inclincations (93°, 98° and 108°) for the detection of geostrophic current vectors above 20° latitude. The second choice is 98° orbit inclination. The relationship shown by Equation (4.37) as

$$V_R = C\ V$$

where V_R is the true local geostrophic current speed, V is the geostrophic current speed evaluated with the RMS noise, and C is a coefficient can be used to study the possible accuracy of recovering geostrophic current velocities from satellite radar altimeter measurements

of varying precision and in different orbits.

The uncertainty in geostrophic current velocity determination is a function of the altimeter along-track slope measurement precision. Altimeter slope measurement uncertainty must be less than 0.1 $\widehat{\text{sec}}$ to achieve a minimum uncertainty in geostrophic current speed determination of 5 cm/sec.

ACKNOWLEDGEMENT

The authors would like to thank Mr. J.T. McGoogan of NASA Wallops Flight Center, Dr. J. Mueller of NASA Goddard Space Flight Center, and Drs. B. Chovitz and B. Douglas of NOAA National Oceanic Survey for their valuable suggestions. Thanks are also due to Mrs. M. Thompson for her typing and Mrs. J. Ware for her drawing.

REFERENCES

Cutting, E., Borne, G., Frautnick, J., McLaughlin, W., Neilson, R., and Thielen, J., Mission for SEASAT-A and Oceanographic Satellite, Jet Propulsion Laboratory Document 622-22, 1977.

Davies, K., Ionospheric Radio Propagation, National Bureau of Standards Monograph 80, Department of Commerce, 1965.

Doodson, A.T., Oceanic Tides, Advances In Geophysics, V.5, Academic Press, N.Y., 1958

Huang, N.E., Leitao, C.D., and Parra, C.G., Large-Scale Gulf Stream Frontal Study Using GEOS-3 Radar Altimeter Data, Journal of Geophysical Research, V.83, No. C9, 4673-4682, 1978.

McGoogan, J.T., and Walsh, E.J., Real-time Determination of Geophysical Parameters from a Multi-Beam Altimeter, AIAA/NASA Conference on "Smart Sensors", Hampton, Va., Nov 1978.

Neumann, G., Pierson, W.J., Jr., Principles of Physical Oceanography, Prentice-Hall, Inc., 1966.

Saatamoinen, J., Atmospheric Corrections for the Troposhere and Stratosphere in Radio Ranging of Satellites, The Use of Artificial Satellites for Geodesy, Geophysical Monography 15, American Geophysical Union, 247-251, 1971.

Sokolnikoff, I.S., Tensor Analysis: Theory and Applications, John Wiley, New York, 1951.

Stoker, J.J., Water Waves, Interscience, N.Y., 1957.

Stommel, H., The Gulf Stream: A Physical and Dynamical Description, University of California Press, 1966.

Stommel, H., and Yoshida, K., Kuroshio: Physical Aspects of the Japan Current, University of Washington Press, 1972.

Sverdrup, H.U., Johnson, M.W., and Fleming, R.H., The Oceans: Their Physics, Chemistry, and Their General Biology, Prentice-Hall, 1946.

Thomas, J., Skagga, G., and Lloyd, J., A Global Ionospheric Model, Report 8321, the Naval Research Laboratory, 1979

Wunsch, C., Determining the General Circulation of the Oceans: A Preliminary Discussion, Science, V. 196, 871-875, 1977